



Space Weather

RESEARCH ARTICLE

10.1002/2016SW001585

Special Section:

Reprise of 2001 Space Weather Monograph

Key Points:

- Two empirical K_p models with high prediction accuracy are presented
- Solar wind-magnetosphere coupling functions are optimized and utilized to achieve best prediction of K_p
- Magnetosphere's response time to external solar wind is investigated and incorporated to improve the models

Correspondence to:

S. Liu,
liusq@nssc.ac.cn

Citation:

Luo, B., S. Liu, and J. Gong (2017), Two empirical models for short-term forecast of K_p , *Space Weather*, 15, 503–516, doi:10.1002/2016SW001585.

Received 7 DEC 2016

Accepted 28 FEB 2017

Accepted article online 4 MAR 2017

Published online 14 MAR 2017

Two empirical models for short-term forecast of K_p

B. Luo^{1,2}, S. Liu^{1,2} , and J. Gong¹

¹National Space Science Center, Chinese Academy of Sciences, Beijing, China, ²School of Astronomy and Space Science, University of Chinese Academy of Sciences, Beijing, China

Abstract In this paper, two empirical models are developed for short-term forecast of the K_p index, taking advantage of solar wind-magnetosphere coupling functions proposed by the research community. Both models are based on the data for years 1995 to 2004. Model 1 mainly uses solar wind parameters as the inputs, while model 2 also utilizes the previous measured K_p value. Finally, model 1 predicts K_p with a linear correlation coefficient (r) of 0.91, a prediction efficiency (PE) of 0.81, and a root-mean-square (RMS) error of 0.59. Model 2 gives an r of 0.92, a PE of 0.84, and an RMS error of 0.57. The two models are validated through out-of-sample test for years 2005 to 2013, which also yields high forecast accuracy. Unlike in the other models reported in the literature, we are taking the response time of the magnetosphere to external solar wind at the Earth explicitly in the modeling. Statistically, the time delay in the models turns out to be about 30 min. By introducing this term, both the accuracy and lead time of the model forecast are improved. Through verification and validation, the models can be used in operational geomagnetic storm warnings with reliable performance.

1. Introduction

K_p is an index to indicate the global geomagnetic activity. It was introduced by *Bartels* [1949] and was calculated as the average of weighted K indices at 13 ground-based magnetic observatories located between 48° and 60° magnetic latitude in the subauroral region. The values of K_p vary from 0 to 9 in thirds and therefore resulting in 28 discrete levels of 0, 0+, 1−, 1, 1+, 2−, 2, ... 9−, 9.

Very often K_p is not considered proper to represent the global geomagnetic activity, since the stations used to determine K_p are limited (13 stations) and are not densely and evenly distributed over the world. However, due to historical reasons, K_p is still widely used in either research or operational communities to scale the global geomagnetic disturbance. Based on K_p , the NOAA Space Weather Prediction Center (SWPC) issues geomagnetic storm alerts when K_p reaches 5 or greater. Similar warning or alert methods are adopted in most space weather operations centers such as the members of the International Space Environment Services.

Due to the algorithms employed to remove the quiet-day curves for the geomagnetic stations and other processing delays, the official values of K_p are published with a few weeks' delay. Such delay makes it useless in real-time geomagnetic storm alerts, though it has little effect for space physics research.

To meet the operational requirements for K_p , one approach is to develop algorithms to estimate the values of K_p , either from local geomagnetic stations owned by an individual space weather center or from network of global geomagnetic stations through international collaboration. Representatives of such algorithms are those developed by *Gehred et al.* [1995] and *Takahashi et al.* [2001]. The algorithm developed by *Gehred et al.* [1995] was reported to be used by the United States Air Force (USAF) 55th Space Weather Squadron, and the algorithm developed by *Takahashi et al.* [2001] has been used by the NOAA SWPC based on a network of contributing stations through cooperative efforts between the SWPC and data provider partners. The GFZ Potsdam, Germany, the official supplier of K_p index, also provides quick-look K_p index in near-real time.

Another approach is to develop forecast models of K_p . The representatives of such models include the Costello model [Costello, 1997], the APL models [Wing et al., 2005], the Bala models [Bala et al., 2009; Bala and Reiff, 2012], and the NARX models [Ayala Solares et al., 2016], most of which are based on artificial neural network algorithms. The main inputs of the models are solar wind parameters, either primitive variables (solar wind speed, interplanetary magnetic field (IMF), density, etc.) or physics-based variables (such as the Boyle Index $\Phi = 10^{-4}v^2 + 11.7B \sin^3(\theta_c/2)$, and the Newell Function $d\Phi_{MP}/dt = v^{4/3}B_T^{2/3} \sin^{8/3}(\theta_c/2)$ used in the Bala

models, where v is the solar wind speed, B is the strength of the IMF, B_T is the magnitude of the IMF vector in the GSM YZ plane, and θ_c is the IMF clock angle which can be calculated as $\theta_c = -(\arccos(-B_z/B_T) - \pi)/2$. The Advanced Composition Explorer (ACE) spacecraft located upstream at Lagrangian point (L1) provides the needed solar wind measurements. These authors developed K_p models with different lead times. For instance, the APL models produce hourly and 4-hourly forecasts of the K_p . The Bala models generate 1, 3, and 6 h ahead predictions. The NARX models give 3, 6, 12, and 24 h ahead predictions. But in summary, the performance degrades with increasing lead time. Among these models, K_p can be best predicted approximately 1 h ahead which comes from the transit time of the solar wind from L1 to Earth (the actual forecast lead time varies depending on the solar wind speed). When using solar wind data as the only input, the Costello model predicted K_p with a correlation coefficient of $r = 0.75$ between the forecast and the official values, while the APL model gave $r = 0.84$ (APL model 3), and the Bala model gave $r = 0.852$ (Bala model 3 in *Bala et al. [2009]*). Later in *Bala and Reiff [2012]*, the Bala model 3 was improved and gave $r = 0.88$. These models showed improvements with different degrees when observed K_p at the previous time step was employed as input. The APL model then gave $r = 0.92$ (APL model 1) and the Bala model then gave $r = 0.863$ (Bala model 1 in *Bala et al. [2009]*). The Costello model had been routinely operational at NOAA SWPC before it was replaced by the APL models. The predictions of the APL models can be obtained at the NOAA SWPC website (<http://www.swpc.noaa.gov/products/wing-kp>). The real-time updated predictions of the Bala models are also available online (<http://mms.rice.edu/realtime/forecast.html>.)

The goal of this study is to develop new empirical models of K_p with improved forecasting performance in the following aspects.

1. To improve the forecast accuracy by taking advantage of solar wind-magnetosphere coupling functions provided by research community. Since the most well known solar wind energy coupling function $\varepsilon = vB^2 \sin^4(\theta_c/2)$ [*Perreault and Akasofu, 1978*] was introduced, various combinations of solar wind parameters were repeatedly examined. Over the recent years, several new solar wind-magnetosphere coupling functions were reported, either by statistical analysis [*Lyatsky et al., 2007; Newell et al., 2007, 2008; McPherron et al., 2015; Wang et al., 2015*], global MHD simulation [*Wang et al., 2014*], or by empirical modeling of geomagnetic indices [*Temerin and Li, 2002, 2006; Li et al., 2007; Luo et al., 2013*].
2. To improve the K_p forecast by investigating and taking account of the magnetosphere's response time to external solar wind. Previous K_p models with a forecast lead time of about 1 h (denoted as Δt , which approximately equals to the transit time of the solar wind from L1 to the Earth) always assumed an immediate magnetospheric responses to the external solar wind parameters (e.g., forecast for K_p of 06–09 UT interval is given at 09– Δt UT). Such assumption would degrade the model performance, either in forecast lead time or accuracy.
3. To develop models with explicit formulas rather than in neural network. During the model development, the formulas and associated numerical values of the model parameters are tuned and optimized. Models with explicit formulas can be easily reproduced and used by people. The final results will help to interpret the solar wind-magnetosphere relationship. We try to improve K_p forecast accuracy by incorporating research outcomes into operational modeling.

The remainder of the paper is organized as follows. Section 2 introduces the data used in this study. Section 3 describes the modeling method. Section 4 presents the two K_p models. Section 5 gives verification and validation of the models as well as some discussions. Section 6 provides a summary and concludes the paper.

2. Data

K_p and contemporary solar wind data were used to develop the models. The data of K_p were obtained from the World Data Center for Geomagnetism, Kyoto (<http://wdc.kugi.kyoto-u.ac.jp>). For solar wind, we used 1 min resolution data. They were obtained from the OMNI website (<http://omniweb.gsfc.nasa.gov/>). The OMNI data had already been propagated to the Earth by taking into account the solar wind convection time from the spacecraft to the bow shock. The reason we chose 1 min rather than hourly resolution solar wind data was that we first performed statistical analysis on magnetosphere's response time (denoted as τ) to external solar wind. Then the 1 min solar wind data at Earth were averaged to 3 h (with a lead time of τ to K_p) to predict the K_p index.

The data used in this paper cover the years 1995–2013, divided into two periods: 1995–2004 and 2005–2013. The data for years 1995–2004 were used for model development through rigorous empirical analysis, and the data for years 2005–2013 were used for validation of the models through out-of-sample test.

3. Modeling Method

We have experimented with two models, one mainly driven by solar wind while the other also uses measured K_p at the previous step. We chose a common functional form from solar wind-magnetosphere coupling functions to reflect the solar wind modulation of K_p . The solar wind-magnetosphere coupling function was a product of factors of solar wind speed v , density n , magnitude of the IMF vector in the GSM YZ plane B_T , and interplanetary magnetic field (IMF) clock angle θ_c , each raised to a different power, with the exponents to be free parameters and fitted. Such a functional form reflects the main effects of solar wind parameters on K_p (e.g., solar wind speed which was investigated by Elliott *et al.* [2013]). Linear, power law, and exponential dependences of K_p on the coupling function were tried to obtain the best prediction. Some other effects were also taken into consideration, such as solar wind viscosity, temporal variations of geomagnetic activity, ionospheric ionization effect of solar ultraviolet (UV) radiation, etc.

As mentioned earlier, the 1 min resolution OMNI solar wind data were averaged to 3 h resolution, but with a lead time τ to the predicted 3 h K_p . This lead time τ reflects the average time lag of geomagnetic activities to solar wind disturbances at the magnetopause. The τ , together with the propagation time Δt of the solar wind from the L1 point to the Earth, determines the total lead time of the model forecast when predicting K_p using solar wind measurements at the L1 point (where the ACE and DSCOVR satellites provide in situ solar wind measurement in real time). The τ was also set as free parameter in the models and fitted.

In handling the gaps of the 1 min resolution OMNI data, to ensure the reliability of the 3 h averages of the solar wind data, at least $N = 120$ points (2/3 of the total 180 points) of the 1 min data were required for each 3 h interval. In the end we had 25,298 3 h samples (86.6% of the total 29,224) left for years 1995–2004, and 22,606 samples (86.0% of the total 26,296) for years 2005–2013, respectively.

The parameters of the models were found by minimizing the root-mean-square (RMS) error between the model and the measured indices, based on the solar wind data and official K_p for the years of 1995–2004, which covers the minimum of solar cycle 22 and almost the whole solar cycle 23. The process of root square minimization was similar to that of the AU, AL, and AE modeling in Luo *et al.* [2013]. We changed the functional forms and parameters back and forth to reduce the RMS error. In the end we arrived at the present result.

4. K_p Models

4.1. Model 1 That Inputs Solar Wind

4.1.1. Description of Model 1

The K_p index is calculated in three steps: (1) A preliminary estimation of K_p related to solar wind; (2) the time modulation of K_p ; (3) the adjustment of K_p related to the solar ultraviolet intensity. Each step consists of one or more explicit equations. The parameters in all these formulas are optimized as a whole rather than step by step.

The preliminary estimation of K_p , denoted as K_p^* , is calculated using solar wind parameters. The pair of solar wind-magnetosphere coupling functions reported by Newell *et al.* [2008], the merging term $d\Phi_{MP}/dt = v^{4/3}B_T^{2/3}\sin^{8/3}(\theta_c/2)$ and the viscous term $n^{1/2}v^2$, provided a starting point in the modeling, but the coefficients were set as free parameters and were optimized in the model. We also tried other functional forms to improve the model. At last the merging term changed to the form of $n^{0.24}v^{1.47}B_T^{0.86}[\sin^{2.70}(\theta_c/2) + 0.25]$ given by Wang *et al.* [2014], while the form of the viscous term remained unchanged. Finally, the optimum terms came out to be $n^{0.084}v^{1.428}B_T^{0.690}(\sin^{5.497}(\theta_c/2) + 0.155)$ and $n^{0.489}v^{2.070}$ as shown in the following model equations, respectively, and K_p^* is the sum of their exponential and linear fittings. The formulas to calculate K_p^* is given as

$$K_p^*(t) = 6.713 - 3.847 \cdot e^{-5.493 \times 10^{-5} \cdot M_{itg}} + 3.955 \times 10^{-5} \cdot M_{itg} - 4.191 \cdot e^{-8.086 \times 10^{-7} \cdot V_{itg}} - 1.920 \times 10^{-7} \cdot V_{itg}, \quad (1)$$

where

$$M_{\text{itg}} = M_{\text{term}}(t - \tau) + 0.273 \times M_{\text{term}}(t - \tau - 0.125),$$

$$V_{\text{itg}} = V_{\text{term}}(t - \tau) + 0.273 \times V_{\text{term}}(t - \tau - 0.125),$$

$$\tau = 0.021,$$

$$M_{\text{term}} = n^{0.084} v^{1.428} B_T^{0.690} (\sin^{5.497}(\theta_c/2) + 0.155),$$

$$V_{\text{term}} = n^{0.489} v^{2.070}.$$

The time tag t associated with the Kp value is the end point of its 3 h interval, in unit of float days since 1995. M_{itg} and V_{itg} are linear integration of M_{term} and V_{term} for the previous two time steps ($t - \tau$ and $t - \tau - 0.125$), respectively. The constant τ of 0.021 (30 min) reflects the optimized magnetosphere's response time to external solar wind. This means that in the model the 3 h averaged solar wind data at Earth leads Kp in $\tau = 0.021$. This also means that on the basis of solar wind observations at the L1 point, Kp can be forecasted $\Delta t + \tau$ ahead, where Δt represents the propagation time of the solar wind from L1 to the Earth (e.g., forecast for Kp of 06–09 UT interval is given at 09 – $\Delta t - \tau$ UT). Compared to previous Kp models, the forecast lead time is extended by $\tau = 30$ min. Considering that current Kp models with best performance predicts Kp in about 1 h advance, such extension of lead time is clearly an improvement. To be compared with, on active times it takes about 30 min for the solar wind with a speed of 900 km/s to travel from the L1 point to the Earth.

Time modulation was introduced considering that annual and universal time variations of geomagnetic indices have been proved to exist [e.g., Cliver *et al.*, 2000; Nagatsuma, 2006, and references therein]. After optimizing the model, the semidiurnal variation of Kp was shown to be negligible. Finally, the preliminarily calculated Kp^* is then modulated by semiannual and diurnal variation of $\sin \phi$ and an annual variation, given as

$$Kp^{**}(t) = Kp^*(t) \cdot \sin^{1.311} \phi(t) \cdot (1 + 0.017 \cdot \sin(fy \cdot t + 4.360)), \quad (2)$$

$$\begin{aligned} \cos \phi(t) &= \sin(fy \cdot t + 0.118) \cdot 0.0224 \cdot \sin(2\pi \cdot t - fy \cdot t + 1.967) \\ &\quad + \cos(fy \cdot t + 0.118) \cdot ((0.39 + 0.0244 \cdot \cos(2\pi \cdot t - fy \cdot t + 1.967))), \end{aligned}$$

where $fy = 2\pi/365.24$ and $\sin \phi$ is nominally the sine of the angle between the magnetic dipole axis and the Sun-Earth line ($\sin \phi = \sqrt{1 - \cos^2 \phi}$ where $\cos \phi$ is calculated as the listed equation) [Temerin and Li, 2002, 2006; Li *et al.*, 2007; Luo *et al.*, 2013]. Similar to the approach for auroral electrojet modeling used in Luo *et al.* [2013], for the Kp model, the optimized revolution angle of the Earth around the Sun, the rotation angle of the Earth, and the magnitude of the offset of the dipole axis from the rotation axis are 0.118 radians, 1.967 radians, and 0.024 radians (reflected by the value 0.0224 and 0.0244), respectively. The term $\sin^{1.311} \phi(t)$ provides for the equinoctial effects, maximum near the equinoxes and minimum at the solstices [Russell and McPherron, 1973; Cliver *et al.*, 2000; Temerin and Li, 2002, 2006; Li *et al.*, 2007; Luo *et al.*, 2013]. The modulation due to this term, $\sin^{1.311} \phi(t)$ used in equation (2), is illustrated in Figure 1a. Note that there is also a diurnal variation due to this term, which corresponds to an offset of the magnetic dipole from the rotation axis by 1.40° (0.024 radians) instead of the actual 11°. Considering that the Kp index was designed to be a planetary index, the resulting Kp should then have no universal time variation at all. But as pointed out by Michel [1964] and manifested in Svalgaard [1976], this goal was not quite achieved and a very small residual universal time variation is still present, which is due to imperfections in the standardization tables used in the computation of Kp by using K indices. The magnitude and phase of the annual variation are reflected by the constants 0.017 and 4.360 in equation (2). The annual phase of 4.360 gives a maximum during the Northern Hemisphere summer months and a minimum during the winter months. In combination, the $\sin^{1.311} \phi(t) \cdot (1 + 0.017 \cdot \sin(fy \cdot t + 4.360))$ term gives an overall time modulation shown in Figure 1b. This is consistent with the auroral electrojet indices models by Luo *et al.* [2013].

Solar ultraviolet radiation can enhance the conductivity of the ionosphere and thus the currents flowing inside it [Nakai and Kamide, 1999; Tobiska *et al.*, 2000; Nagatsuma, 2006; Luo *et al.*, 2013]. As an ultraviolet flux proxy, $F_{10.7}$ reflects the conductivity of the ionosphere through ionization. $F_{10.7}$ is introduced to the model to reflect

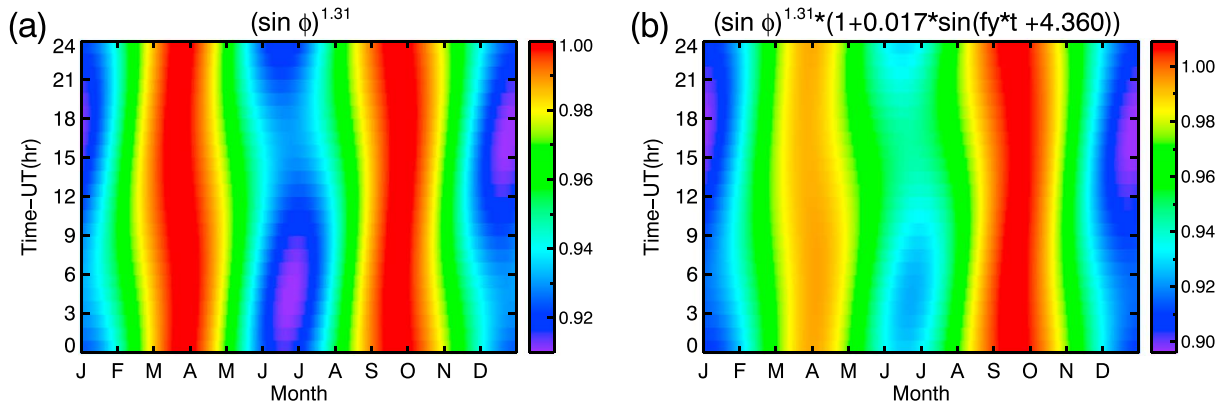


Figure 1. The annual, semiannual, and diurnal time modulations of K_p . (a) Time modulation of K_p by the $\sin^{1.311} \phi(t)$ term. (b) The overall time modulation of K_p by the term $\sin^{1.311} \phi(t) \cdot (1 + 0.017 \cdot \sin(fy \cdot t + 4.360))$.

the effect of solar ultraviolet radiation on K_p . What is more, an offset of -0.568 with $F_{10.7}$ modulation is added to the K_p prediction. It should be pointed out that this is a smaller term compared to the other terms.

$$K_p(t) = K_p^{**}(t) \cdot (1 - 0.536 \times 10^{-3} \cdot F_{10.7}) - 0.568 \times (1 - 4.948 \times 10^{-3} \cdot F_{10.7}). \quad (3)$$

4.1.2. Performance of Model 1

An example of the model output over a randomly selected 1 month interval is shown in Figure 2. Note that the M_{itg} in Figure 2d, V_{itg} in Figure 2e, and the modeled K_p in Figure 2f correspond to the solar wind 30 min

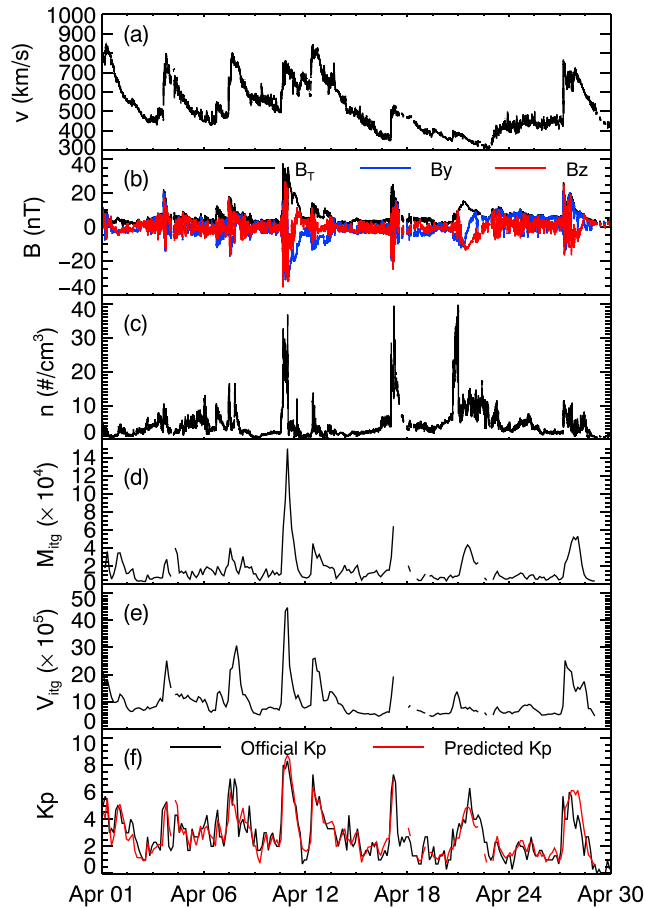


Figure 2. (a–e) Relevant solar wind parameters and (f) a comparison between the predicted K_p (red) from model 1 and the official values (black) for April 2001.

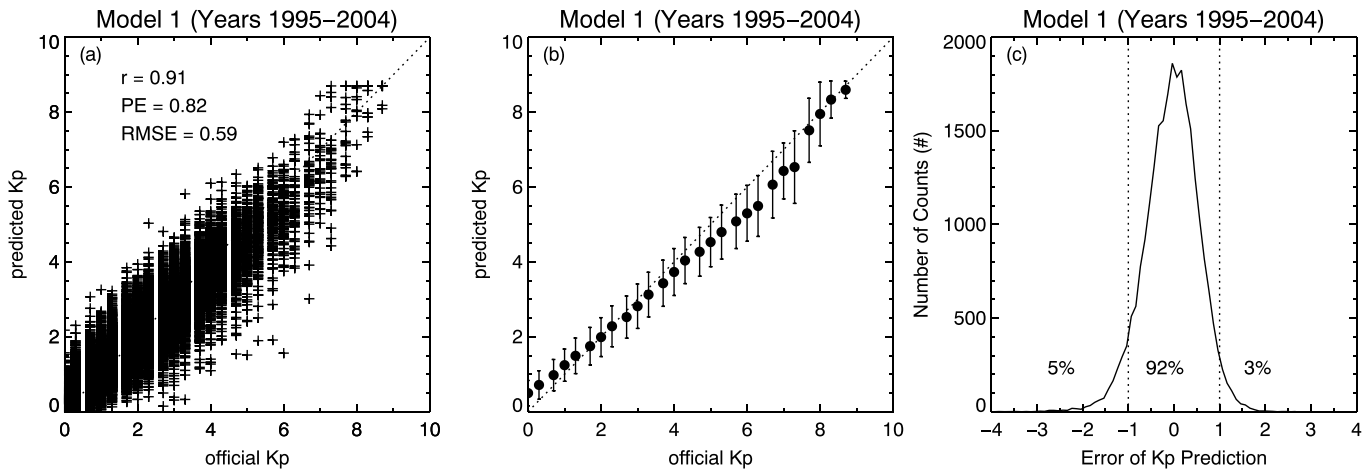


Figure 3. The performance of model 1. (a) The scatter plot of the predicted K_p compared with the official K_p . Official K_p is plotted on the x axis and the model prediction is plotted on the y axis. Perfect predictions would lie on the line with a slope of one. (b) The averages of predicted K_p for each of the 28 discrete levels of the official K_p . The error bars indicate one standard deviation. (c) Illustration of the occurrence distribution of the prediction errors.

to 6.5 h ahead in Figures 2a–2c. It can be seen that the model predictions follow the measurement closely. Figure 3a shows the comparison of the predicted K_p with the official values. For the 10 years of 1995–2004, model 1 gives a linear correlation of $r = 0.91$, a prediction efficiency (PE , defined as $PE = 1 - (\text{mean-squared residual}) / (\text{variance of data})$) of 0.82, and an RMS error of 0.59. The $r = 0.91$ is so far the best result among solar wind driven K_p models reported in literatures. Figure 3b shows the averages of the predicted K_p for each of the 28 discrete levels of the official K_p . The error bars, defined as 1 standard deviation of the predicted values for each level of K_p , are also overplotted. For major geomagnetic activities ($K_p \geq 8$), the errors of the model decrease with the increase of K_p . Similar to those found in Wing et al. [2005], K_p s between 4 and 7 are really harder to predict. Figure 3c shows occurrence distribution of the errors of K_p prediction, where error is calculated as $\text{err} = K_{p\text{predicted}} - K_{p\text{observed}}$. Percentages for $\text{err} < -1.0$, $|\text{err}| \leq 1.0$, and $\text{err} > 1.0$ are also shown, respectively. It can be seen that 92% of K_p can be predicted well with $|\text{err}| \leq 1.0$. Compared with the other models as introduced in section 1, our model yields higher correlation coefficient.

4.2. Model 2 That Inputs Solar Wind and K_p

Model 2 is given in equations (4)–(7). Compared with model 1, the main difference is equation (6), which reflects the influence of precondition of the geomagnetic activity on the next K_p value. Meanwhile, the M_{itg} and V_{itg} terms are now determined by the current step of solar wind, while those in model 1 are determined by the previous two steps. All the coefficients are retuned using data for years 1995–2004 by minimizing the RMS error.

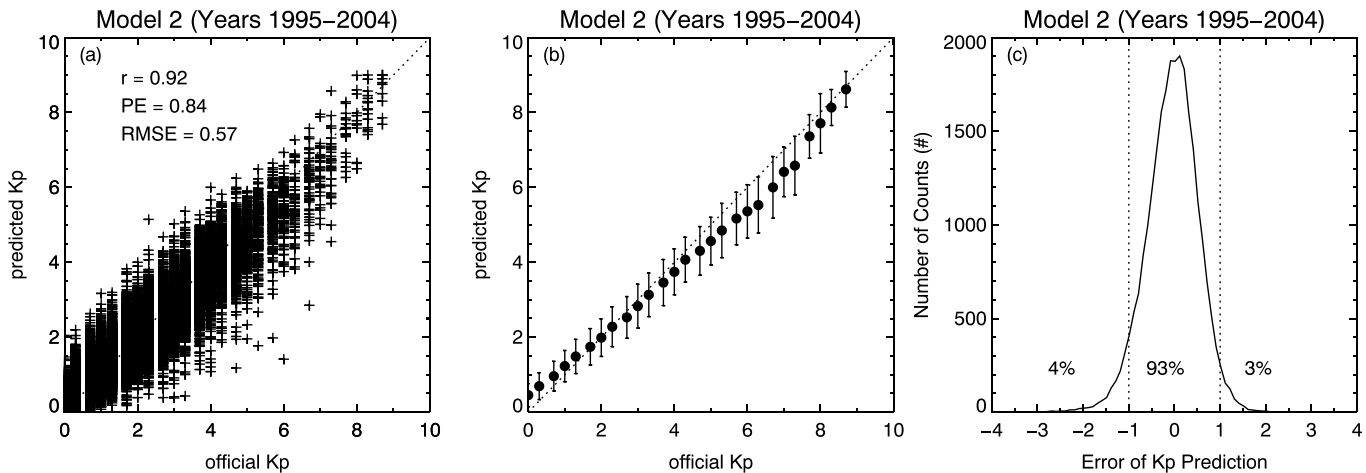


Figure 4. The performance of model 2, shown in the same format as Figure 3.

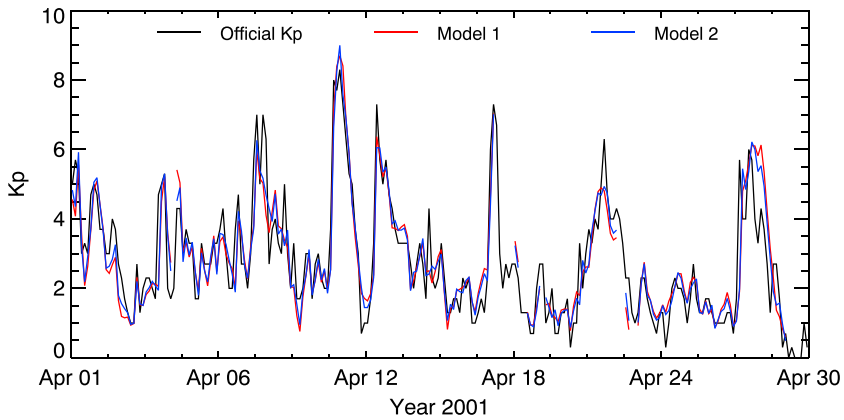


Figure 5. Comparisons between the official K_p (black), the predicted K_p by model 1 (red), and the predicted K_p by model 2 (blue) for April 2001.

Figure 4 summarizes the overall performance of model 2, in the same format as Figure 3. For the 10 years of 1995–2004, model 2 gives a linear correlation of $r = 0.92$, a PE of 0.84, and an RMS error of 0.57. 93% of the predictions have error better than 1.0. The forecast accuracy shows improvement compared with model 1. Figure 5 shows the prediction comparison of the two models with official K_p for April 2001.

It should be noted that in operational services, model 2 requires the availability of nowcast K_p , while model 1 depends mainly on solar wind. This means that given accurate solar wind predictions (rather than in situ observation at L1), model 1 will provide a reliable prediction of K_p by multistep running approach. Model 2 can only be run one step ahead because of its dependence on measured K_p at the previous time step. But currently as the nowcast K_p such as from the SWPC are rather discrete in their quantization and how they are defined, the final outcome of this model in real-time operation is bound to differ from the study here.

$$Kp^*(t) = 5.432 - 4.023 \cdot e^{-5.667 \times 10^{-5} \cdot M_{itg}} + 2.090 \times 10^{-5} \cdot M_{itg} - 2.551 \cdot e^{-1.185 \times 10^{-6} \cdot V_{itg}} - 3.295 \times 10^{-7} \cdot V_{itg}, \quad (4)$$

$$Kp^{**}(t) = Kp^*(t) \cdot \sin^{1.443} \phi(t) \cdot (1 + 0.018 \cdot \sin(fy \cdot t + 4.339)), \quad (5)$$

$$Kp^{***}(t) = Kp^{**}(t) + 0.279 \cdot Kp_{obs}(t - 0.125), \quad (6)$$

$$Kp(t) = Kp^{***}(t) \cdot (1 - 0.536 \times 10^{-3} \cdot F_{10.7}) - 0.568 \times (1 - 4.948 \times 10^{-3} \cdot F_{10.7}), \quad (7)$$

where

$$M_{itg} = M_{term}(t - \tau),$$

$$V_{itg} = V_{term}(t - \tau),$$

$$\tau = 0.021,$$

$$M_{term} = n^{0.082} V^{1.418} B_T^{0.656} (\sin^{5.545} (\theta_c/2) + 0.171),$$

$$V_{term} = n^{0.505} V^{2.060},$$

$$\begin{aligned} \cos \phi(t) = & \sin(fy \cdot t + 0.115) \cdot 0.0272 \cdot \sin(2\pi \cdot t - fy \cdot t + 2.113) \\ & + \cos(fy \cdot t + 0.115) \cdot ((0.39 + 0.0296 \cdot \cos(2\pi \cdot t - fy \cdot t + 2.113)). \end{aligned}$$

5. Discussion

5.1. Out of Sample Comparison for Years 2005–2013

To further verify and validate the accuracy of the models, data for years of 2005–2013 were used for out of sample comparison. Figure 6 shows the comparison of the predicted K_p with the official values, in the same format as Figure 3. Model 1 gives an $r = 0.90$, a PE of 0.81, and an RMS error of 0.55, while model 2 gives an $r = 0.91$, a PE of 0.83, and an RMS error of 0.53. The performances are comparable to that for years 1995–2004 which were used to fit the parameters of the models. The RMS error for years 2005–2013 is smaller than that for years 1995–2004. This may be due to the fact that the geomagnetic activity for years 2005–2013 was relatively quiet compared with 1995–2004. From Figure 6b one may notice the large error bar for $K_p = 8$. This is due to the lack of samples for high geomagnetic disturbances during this period. Only two valid points were left for $K_p = 8$ and one was predicted to be 6 which resulted in the large error. In conclusion, the out of sample verification of the K_p models validates the forecast accuracy of the models.

5.2. Implications on the Solar Wind-Magnetosphere Coupling

As has been mentioned earlier, many solar wind-magnetosphere coupling functions were proposed in research community during the past decades. These coupling functions, similar to the famous ε , are typically a product of factors of solar wind speed v , density n , magnitude of the IMF vector in the GSM YZ plane B_T , and interplanetary magnetic field (IMF) clock angle θ_c , each raised to a different power.

By developing an empirical Dst forecast model with very high accuracy, *Temerin and Li* [2002, 2006] reported the coupling function which can be approximately written as $n^{1/2}v^2B_T \sin^6(\theta_c/2)$. From a simple theoretical consideration, *Lyatsky et al.* [2007] gave a coupling function of $F_\alpha = avB_T^{1/2} \sin^2(\theta_c/2)$ in which a is a coefficient. This function showed high correlation with the polar cap (PC) geomagnetic activity index. *Newell et al.* [2007] developed a universal coupling function $d\Phi_{MP}/dt = v^{4/3}B_T^{2/3} \sin^{8/3}(\theta_c/2)$ which correlates better with all magnetic indices than any other previous coupling function. The linear combination of $d\Phi_{MP}/dt$ with a viscous term $n^{1/2}v^2$ showed the best correlations with most magnetospheric state variables [Newell et al., 2008]. In the AU , AL , and AE forecast models developed by *Luo et al.* [2013], which was an ongoing work of *Li et al.* [2007], $n^{0.39}v^{3.52}B_T^{1.996} \sin^{7.63}(\theta_c/2)$ and $n^{0.23}v^{4.17}B_T^{1.39} \sin^{6.92}(\theta_c/2)$ were reported to be the main driver terms for AU and AL , respectively. *Wang et al.* [2014] reported an energy coupling function of $n^{0.24}v^{1.47}B_T^{0.86}[\sin^{2.70}(\theta_c/2) + 0.25]$ from a global MHD simulation. Later on, *McPherron et al.* [2015] reported an optimum solar wind coupling function of $n^{0.1}v^{1.92}B_T^{0.79} \sin^{3.67}(\theta_c/2)$ which was derived by optimizing the $d\Phi_{MP}/dt$ function through the technique of local linear prediction filters to simultaneously determine the exponents in the coupling function and the prediction filter that transforms it to AL .

It can be clearly seen that the coupling functions could be different when they are optimized for different magnetospheric indices. The coupling functions mentioned above were individually obtained to describe Dst , AU , AL , and PC indices, etc. The exponents for the same solar wind variables in these functions are quite different. What is more, even when the coupling functions were optimized for the same magnetospheric index, the coupling functions could also be different because the authors used different approaches in their study. This can be seen from the coupling functions by *Luo et al.* [2013] and *McPherron et al.* [2015], both of which aimed to describe the geomagnetic index AL .

While the above mentioned coupling functions were obtained by relating solar wind to regional geospace disturbances, until now none was optimized for the global geomagnetic index K_p . This led us to search for such a function through a rigorous empirical statistical modeling of K_p , which, on the one hand, can improve the forecast capability of K_p and, on the other hand, help to understand the solar wind-magnetosphere coupling from another view. The models gave a pair of optimal coupling functions of $n^{0.084}v^{1.428}B_T^{0.690}(\sin^{5.497}(\theta_c/2) + 0.155)$ and $n^{0.489}v^{2.070}$ (the coefficients show very tiny differences between model 1 and model 2). The former one could be referred to as representing the coupling through magnetic reconnections at the magnetopause. The second one, $n^{0.489}v^{2.070}$, could be referred to as the viscous term. The viscous term is almost identical to the one reported by *Newell et al.* [2008]. Our results again support the point of *Newell et al.* [2008] that bringing in the viscous term enhances the predictability of K_p . It also suggests that in order to achieve the best prediction performance, the functional form as well as the parameters of the coupling functions should be optimized for the specific index one intends to forecast.

It is of interest to see how K_p changes with the merging term and the viscous term. From equation (1) in which K_p is preliminarily estimated using the two terms, it is easy to see that K_p will always increase when the merging term increases. Nevertheless, for the viscous term the relationship shows some differences.

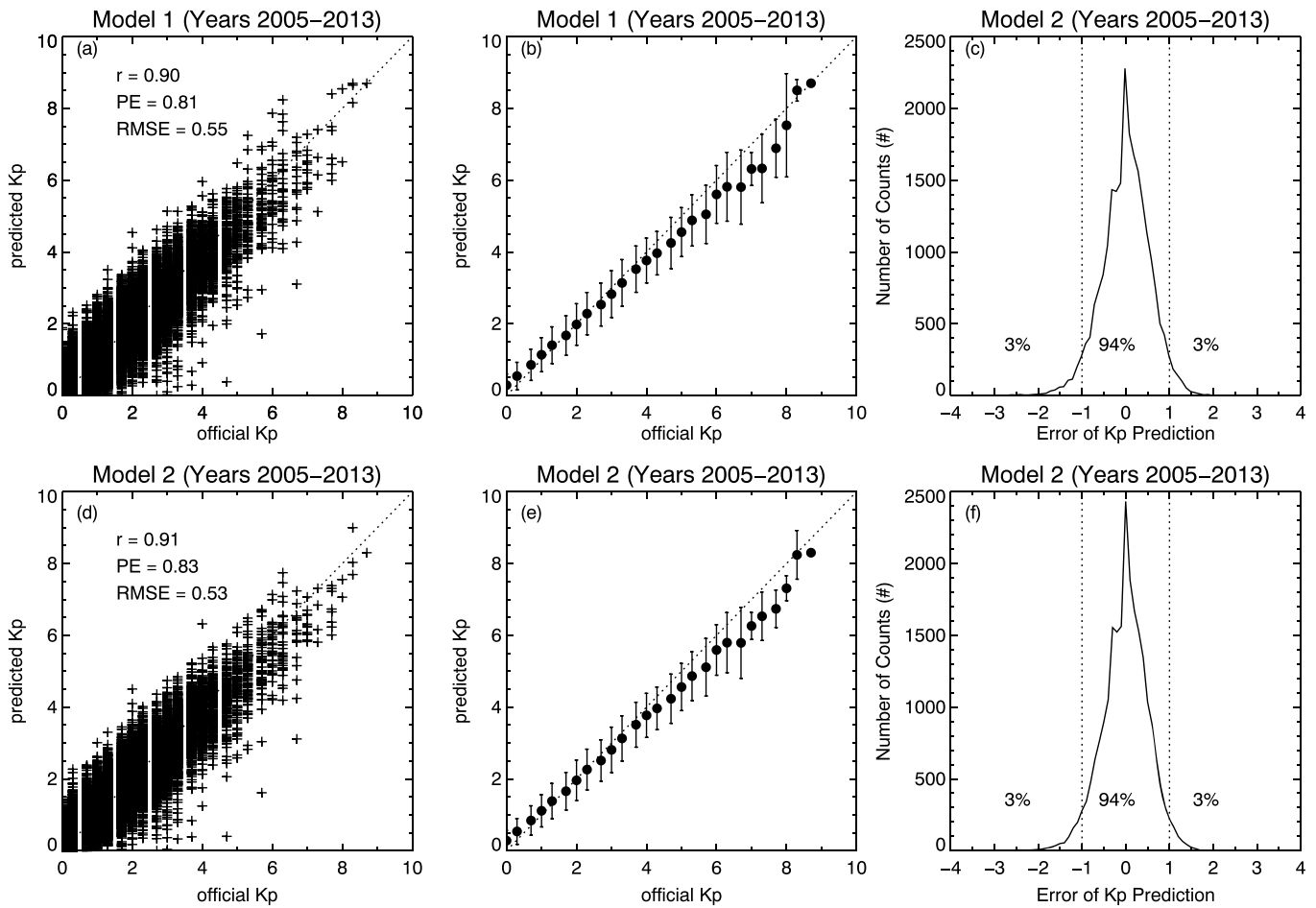


Figure 6. The out-of-sample test of (a–c) model 1 and (d–f) model 2 for years 2005–2013, shown in the same format as Figure 3.

For $V_{itg} < 3.55 \times 10^6$, Kp also increases with V_{itg} , while for $V_{itg} > 3.55 \times 10^6$, Kp tends to decrease with the increase of V_{itg} . We checked how often the condition of $V_{itg} > 3.55 \times 10^6$ occurred during 1995 to 2004. It was found that there were only 33 (0.11% of the total 29,224) samples with values of V_{itg} greater than 3.55×10^6 . On the one hand, this indicates that $V_{itg} > 3.5 \times 10^6$ occurs rather rarely. On the other hand, the percentage is so small that the interpretation must be very careful, since the models were developed by minimizing the RMS error for all the samples. Right now it is hard to conclude whether this feature is a real nature or a mathematical chance of the model. More studies will be needed to figure it out.

5.3. Time Lag of Kp to External Solar Wind

One improvement of the models introduced in this study is the increased lead time of the Kp forecast, by taking into account the time lag of magnetospheric response (thus the geomagnetic activity) to the solar wind and IMF variations at the magnetopause. Such time delay exists in many magnetosphere phenomena and has been investigated and proved by several studies. The plasma sheet plays an important role in magnetospheric activities by connecting the solar wind, outer magnetosphere, and inner magnetosphere. It has been reported that the plasma sheet properties correlate well with solar wind and IMF parameters in hours time lag [e.g., Terasawa *et al.*, 1997; Borovsky *et al.*, 1998; Wing *et al.*, 2006; Wang *et al.*, 2007; Øieroset *et al.*, 2003; Luo *et al.*, 2011]. The time lags are different, depending on the direction of the IMF as well as the location in the plasma sheet. Recently, Rong *et al.* [2015] reported a time delay of 1–1.5 h of the interplanetary magnetic field penetration into the Earth's magnetotail.

The time lag of geomagnetic activity to the solar wind has also been reported by several authors. Through a high time resolution study of interplanetary correlations with AE , Baker *et al.* [1981] reported a time lag of about 40 min of AE to the solar wind parameters. In the Dst models by Temerin and Li [2002, 2006] and AU ,

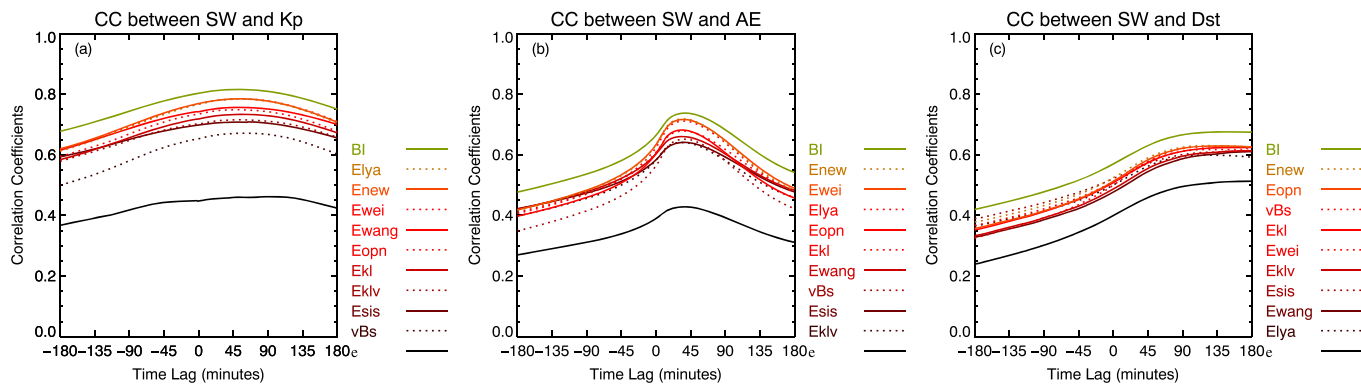


Figure 7. Cross correlations between (a) K_p , (b) AE , (c) Dst and 11 selected solar wind-magnetosphere coupling functions. The coordinate is the correlation coefficient and the abscissa is the number of minutes by which the geomagnetic index lagged the solar wind parameters. On the right of the time-lagged correlation coefficient profiles, the coupling functions are ranked according to their peak correlation coefficients with the geomagnetic index.

Figures 7a–7c show the result of the lagged correlation analysis between 11 selected coupling functions and K_p , AE , and Dst , respectively. In each panel, each line shows a linear cross-correlation result between the geomagnetic index and an individual coupling function with the geomagnetic index lagging the solar wind by -180 min to $+180$ min. The coupling functions are ranked according to their peak correlation coefficients with the geomagnetic index, shown on the right part of the panels. It can be seen that more than 10 coupling functions show high correlation coefficients (r over 0.7) with K_p . The time-lagged correlation coefficient profiles typically show clear, smooth variations as the time lag goes from -180 min to $+180$ min and r reaches a relative peak at time lag of $+30$ min to $+60$ min. For AE and Dst , time lags also exist. In general, averaged time lag for K_p is between AE and Dst . Since our result is based on very large data set covering almost two solar cycles, it is clearly manifested that on average a time lag of $+30$ min to $+60$ min exists between K_p and the solar wind parameters at the magnetopause. Such time lag should be considered in K_p forecast models, on the one hand, to increase the accuracy of the models and, on the other hand, to achieve a longer lead time of prediction.

5.4. Performance of the Models for Geomagnetic Storm Warnings

Nowcast K_p has been used to characterize the magnitude of geomagnetic storms by many operational space weather centers, due to the unavailability of real-time official K_p . Although this will introduce some uncertainty, it is now the best solution to provide real-time space weather service. Several nowcast algorithms have been reported and among these the most popular one was developed by *Takahashi et al. [2001]* which is now routinely operational at the NOAA SWPC. SWPC calculates a near-real-time estimate of the K_p index using a network of about eight contributing stations through cooperative efforts between SWPC and data provider partners, most of which are located in the western hemisphere. These indices may differ from the final official K_p values derived monthly by the GeoForschungsZentrum, Potsdam, Germany, using a network of magnetometers.

One natural question is: whether K_p forecast models are reliable for operational space weather centers to issue geomagnetic storm warnings? Compared with the alerts based on nowcast K_p , an obvious advantage of using forecast model is that it gives longer lead time. But how about the reliability (accuracy) of such warnings? To answer this question, we evaluated the performance of model 1 by comparing it with the nowcast K_p of NOAA SWPC.

For operational geomagnetic storm alert, K_p estimates are rounded to the nearest whole numbers (i.e., 1, 2, ..., 8, 9). So, predicted K_p of model 1 and the contemporary official K_p were rounded to the nearest whole numbers to perform the comparison. Data of nowcast K_p are available from 1997 on the SWPC website, and the comparison here covers the years 1997–2013.

The results are shown in Figure 8. Figures 8a–8c show comparison between model 1 and the official K_p . Figure 8a shows the occurrence frequency of the forecast and the corresponding official values. Figure 8b shows the Glyph scatterplot of the bivariate frequency distribution of the forecast and official K_p . The Glyph

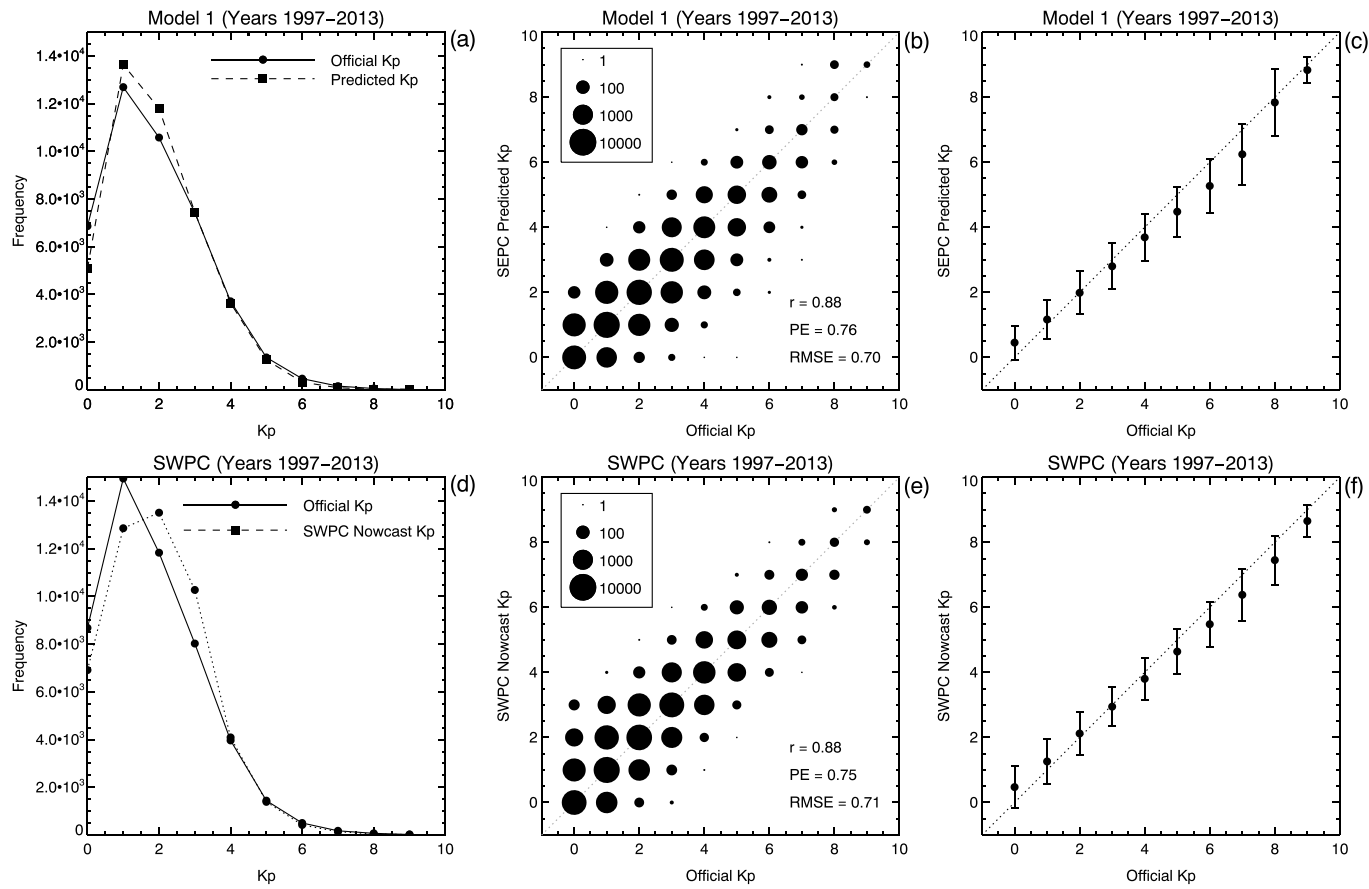


Figure 8. Comparisons of the predicted K_p by model 1 and the NOAA SWPC nowcast K_p with the official values for years 1997–2013. The K_p values have been rounded to the nearest whole numbers which are commonly used for scales of geomagnetic storms in operations centers. (a) The occurrence frequency of the predicted K_p compared with that of the official K_p . (b) The Glyph scatterplot of the bivariate frequency distribution of the predicted K_p and the official values. The circular glyphs have been scaled to have areas proportional to the log of the counts. (c) The averages of the predicted K_p for each of the 10 discrete levels of the rounded official K_p , with the error bars defined as 1 standard deviation. (d–f) Comparisons between the NOAA SWPC nowcast K_p and the official values, which have the same formats as Figures 8a–8c, respectively.

scatterplot is an extension of the ordinary scatterplot, in which the simple dots locating points on the two-dimensional plane defined by two variables are replaced by “glyphs” that encode the values of additional variables in their sizes and/or shapes. Here the circular glyphs have been scaled to have areas proportional to the log of the counts. Figure 8c shows the averages of the K_p forecast for each of the 10 discrete levels of the rounded official K_p , with the error bars defined as 1 standard deviation of the predicted values. Figures 8d–8f show the comparison between the SWPC nowcast K_p and the corresponding official values, in the same formats as Figures 8a–8c, respectively. It should be noted that the number of samples for the model is less than that for the SWPC nowcast K_p , due to the gaps in the solar wind. Comparing Figures 8a and 8d, one can see that both model 1 and SWPC nowcast method yield similar distribution of K_p comparable to the official values, but on average the model tends to overestimate K_p for observed values of 1 and 2, while the SWPC nowcast K_p tends to overestimate K_p for observed values of 2 and 3. Comparing Figures 8b and 8e, model 1 and the SWPC nowcast method give almost the same statistical results of linear correlation coefficient with official K_p ($r = 0.88$), prediction efficiency ($PE = 0.76$), and RMS error (RMS error = 0.70). From Figures 8e and 8f, the errors of the model and the SWPC nowcast K_p are comparable, with the latter showing slight better performance for severe ($K_p = 7, 8$) geomagnetic storms.

From the out-of-sample verification, as well as the comparison with the commonly used nowcast algorithm of K_p , the models of K_p can be used in operational geomagnetic storm warnings with acceptable reliability. Compared with the near-real-time alerts based on the nowcast K_p , the models enable an extension of 1.5 h lead time of warning given continuous and reliable upstream solar wind measurement at the L1 point.

6. Summary

We developed two empirical models to predict the K_p index. The models' parameters were obtained by minimizing the root-mean-square (RMS) error between the prediction and the official values for years 1995–2004. Model 1 mainly inputs solar wind parameters, while model 2 uses measured K_p in addition. Model 1 gave a linear correlation of $r = 0.91$ between the modeled K_p and the official values, a prediction efficiency (PE) of 0.82, and an RMS error of 0.59. Model 2 gave an $r = 0.92$, a PE of 0.84, and an RMS error of 0.57. Out-of-sample test of these models for years 2005–2013 achieved almost the same scores which validated their accuracy. Compared with previous models of K_p , our models are at the top levels as reflected by the evaluation metrics. Compared with neural network-based models which have also achieved considerable successes, an advantage of models with explicit formulations (such as those by Ayala Solares *et al.* [2016] and the models in this paper) is that they can be easily reproduced by readers. These models can be used as a benchmark against which other methods can be measured.

The final models gave a pair of coupling functions $n^{0.084}v^{1.428}B_T^{-0.690}(\sin^{5.497}(\theta_c/2)+0.155)$ and $n^{0.489}v^{2.070}$ that can best predict the K_p index. Comparing them with those proposed in published literatures, the exponents of these functions are different. A possible interpretation is that these functions are based on different geospace indices. This implies that in empirical modeling of geospace indices, the coupling function need to be tuned for specific index to obtain the best accuracy.

We statistically investigated the magnetosphere's response time to external solar wind at Earth and incorporated it into the K_p modeling. The response time appeared to be 30 min. This improves the accuracy of the models as well as the forecast lead time. It is recommended that the time lag of magnetospheric responses to the solar wind disturbances at the magnetopause should be considered in future researches, either in physics study or forecast modeling.

Model 1 was further evaluated for operational geomagnetic storm warnings and was compared with the performance of the NOAA SWPC nowcast K_p , which is now widely used in near-real-time geomagnetic storm alerts by many operations centers around the world. It shows that the model has similar accuracy to the NOAA SWPC nowcast K_p . This suggests that given a continuous and reliable solar wind measurement at the L1 point, the model can be used in geomagnetic storm warnings with no degradation compared with the nowcast approach, but with about 1.5 h lead time which is valuable for operations centers.

Acknowledgments

We wish to thank the GeoForschungsZentrum (GFZ), Potsdam, Germany and the World Data Center for Geomagnetism, Kyoto (<http://wdc.kugi.kyoto-u.ac.jp>) for maintaining and providing the official K_p records. The OMNI data were obtained from the GSFC/SPDF OMNIWeb interface at <http://omniweb.gsfc.nasa.gov>. This work was mainly supported by NNSFC grant 41474164. The author B. Luo is also supported by the Youth Innovation Promotion Association, Chinese Academy of Sciences.

References

- Ayala Solares, J. R., H.-L. Wei, R. J. Boynton, S. N. Walker, and S. A. Billings (2016), Modeling and prediction of global magnetic disturbance in near-Earth space: A case study for K_p index using NARX models, *Space Weather*, 14, 899–916, doi:10.1002/2016SW001463.
- Baker, D. N., E. W. Hones Jr., J. B. Payne, and W. C. Feldman (1981), A high time resolution study of interplanetary parameter correlations with AE, *Geophys. Res. Lett.*, 8(2), 179–182, doi:10.1029/GL008i002p00179.
- Bala, R., and P. Reiff (2012), Improvements in short-term forecasting of geomagnetic activity, *Space Weather*, 10, S06001, doi:10.1029/2012SW000779.
- Bala, R., P. H. Reiff, and J. E. Landivar (2009), Real-time prediction of magnetospheric activity using the Boyle index, *Space Weather*, 7, S04003, doi:10.1029/2008SW000407.
- Bartels, J. (1949), The standardized index, K_s , and the planetary index, K_p , *IATME Bull.*, 12b, 97–120.
- Borovsky, J. E., M. F. Thomsen, R. C. Elphic, T. E. Cayton, and D. J. McComas (1998), The transport of plasma sheet material from the distant tail to geosynchronous orbit, *J. Geophys. Res.*, 103(A9), 20,297–20,331, doi:10.1029/97JA03144.
- Boyle, C. B., P. H. Reiff, and M. R. Hairston (1997), Empirical polar cap potentials, *J. Geophys. Res.*, 102, 111–126, doi:10.1029/96JA01742.
- Burton, R. K., R. L. McPherron, and C. T. Russell (1975), An empirical relationship between interplanetary conditions and Dst , *J. Geophys. Res.*, 80(31), 4204–4214, doi:10.1029/JA080i031p04204.
- Chapman, S., and V. C. A. Ferraro (1931), A new theory of magnetic storms, *Terr. Magn. Atmos. Electr.*, 36, 77–97, doi:10.1029/TE036i002p00077.
- Cliver, E. W., Y. Kamide, and A. G. Ling (2000), Mountains versus valleys: Semiannual variation of geomagnetic activity, *J. Geophys. Res.*, 105(A2), 2413–2424, doi:10.1029/1999JA900439.
- Costello, K. A. (1997), Moving the Rice MSFM into a real-time forecast mode using solar wind driven forecast modules, PhD thesis, Rice Univ., Houston, Tex.
- Crooker, N. U., J. Feynman, and J. T. Gosling (1977), On the high correlation between long-term averages of solar wind speed and geomagnetic activity, *J. Geophys. Res.*, 82, 1933–1937, doi:10.1029/JA082i013p01933.
- Dungey, J. W. (1961), Interplanetary magnetic field and the auroral zones, *Phys. Rev. Lett.*, 6, 47–48, doi:10.1103/PhysRevLett.6.47.
- Elliott, H. A., J.-M. Jahn, and D. J. McComas (2013), The K_p index and solar wind speed relationship: Insights for improving space weather forecasts, *Space Weather*, 11, 339–349, doi:10.1002/swe.20053.
- Gehred, P. A., W. Clifswallow, and J. D. Schroeder III (1995), A comparison of USAF Ap and K_p indices to Göttingen indices, Tech. Memo. ERL SEL-88, NOAA, Silver Spring, Md.
- Kan, J. R., and L. C. Lee (1979), Energy coupling function and solar wind-magnetosphere dynamo, *Geophys. Res. Lett.*, 6, 577–580, doi:10.1029/GL006i007p00577.
- Li, X., K. S. Oh, and M. Temerin (2007), Prediction of the AL index using solar wind parameters, *J. Geophys. Res.*, 112, A06224, doi:10.1029/2006JA011918.

- Luo, B., W. Tu, X. Li, J. Gong, S. Liu, E. Burin des Roziers, and D. N. Baker (2011), On energetic electrons (>38 keV) in the central plasma sheet: Data analysis and modeling, *J. Geophys. Res.*, **116**, A09220, doi:10.1029/2011JA016562.
- Luo, B., X. Li, M. Temerin, and S. Liu (2013), Prediction of the AU, AL, and AE indices using solar wind parameters, *J. Geophys. Res. Space Physics*, **118**, 7683–7694, doi:10.1002/2013JA019188.
- Lyatsky, W., S. Lyatskaya, and A. Tan (2007), A coupling function for solar wind effect on geomagnetic activity, *Geophys. Res. Lett.*, **34**, L02107, doi:10.1029/2006GL027666.
- McPherron, R. L., T.-S. Hsu, and X. Chu (2015), An optimum solar wind coupling function for the AL index, *J. Geophys. Res. Space Physics*, **120**, 2494–2515, doi:10.1002/2014ja020619.
- Michel, F. C. (1964), K_p as a planetary index, *J. Geophys. Res.*, **69**(19), 4182–4183, doi:10.1029/JZ069i019p04182.
- Nagatsuma, T. (2006), Diurnal, semiannual, and solar cycle variations of solar wind-magnetosphere-ionosphere coupling, *J. Geophys. Res.*, **111**, A09202, doi:10.1029/2005JA011122.
- Nakai, H., and Y. Kamide (1999), Solar cycle variations in the storm-substorm relationship, *J. Geophys. Res.*, **104**, 22,695–22,700, doi:10.1029/1999JA900278.
- Newell, P. T., T. Sotirelis, K. Liou, C.-I. Meng, and F. J. Rich (2007), A nearly universal solar wind-magnetosphere coupling function inferred from 10 magnetospheric state variables, *J. Geophys. Res.*, **112**, A01206, doi:10.1029/2006JA012015.
- Newell, P. T., T. Sotirelis, K. Liou, and F. J. Rich (2008), Pairs of solar wind-magnetosphere coupling functions: Combining a merging term with a viscous term works best, *J. Geophys. Res.*, **113**, A04218, doi:10.1029/2007JA012825.
- Øieroset, M., T. D. Phan, M. Fujimoto, L. Chan, R. P. Lin, and R. Skoug (2003), Spatial and temporal variations of the cold dense plasma sheet: Evidence for a low-latitude boundary layer source?, in *Earth's Low-Latitude Boundary Layer*, edited by P. T. Newell and T. Onsager, pp. 253–264, AGU, Washington, D. C.
- Perreault, P., and S.-I. Akasofu (1978), A study of geomagnetic storms, *Geophys. J. Int.*, **54**, 547–573, doi:10.1111/j.1365-246X.1978.tb05494.x.
- Rong, Z. J., A. T. Y. Lui, W. X. Wan, Y. Y. Yang, C. Shen, A. A. Petrukovich, Y. C. Zhang, T. L. Zhang, and Y. Wei (2015), Time delay of interplanetary magnetic field penetration into Earth's magnetotail, *J. Geophys. Res. Space Physics*, **120**, 3406–3414, doi:10.1002/2014JA020452.
- Russell, C. T., and R. L. McPherron (1973), Semiannual variation of geomagnetic activity, *J. Geophys. Res.*, **78**(1), 92–108, doi:10.1029/JA078i001p00092.
- Scurry, L., and C. T. Russell (1991), Proxy studies of energy transfer to the magnetosphere, *J. Geophys. Res.*, **96**, 9541–9548, doi:10.1029/91JA00569.
- Svalgaard, L. (1976), Recalibration of Bartels' geomagnetic activity indices K_p and ap to include universal time variations, *J. Geophys. Res.*, **81**, 5182–5188, doi:10.1029/JA081i028p05182.
- Takahashi, K., B. A. Toth, and J. V. Olson (2001), An automated procedure for near-real-time K_p estimates, *J. Geophys. Res.*, **106**(A10), 21,017–21,032, doi:10.1029/2000JA000218.
- Temerin, M., and X. Li (2002), A new model for the prediction of Dst on the basis of the solar wind, *J. Geophys. Res.*, **107**(A12), 1472, doi:10.1029/2001JA007532.
- Temerin, M., and X. Li (2006), Dst model for 1995–2002, *J. Geophys. Res.*, **111**, A04221, doi:10.1029/2005JA011257.
- Terasawa, T., et al. (1997), Solar wind control of density and temperature in the near-Earth plasma sheet: WIND/GEOTAIL collaboration, *Geophys. Res. Lett.*, **24**(8), 935–938, doi:10.1029/96GL04018.
- Tobiska, W. K., T. Woods, F. Eparvier, R. Viereck, L. Floyd, D. Bouwer, G. Rottman, and O. R. White (2000), The SOLAR2000 empirical solar irradiance model and forecast tool, *J. Atmos. Sol. Terr. Phys.*, **62**, 1233–1250, doi:10.1016/S1364-6826(00)00070-5.
- Vasyliunas, V. M., J. R. Kan, S.-I. Akasofu, and G. L. Siscoe (1982), Scaling relations governing magnetospheric energy transfer, *Planet. Space Sci.*, **30**, 359–365, doi:10.1016/0032-0633(82)90041-1.
- Wang, C., J. P. Han, H. Li, Z. Peng, and J. D. Richardson (2014), Solar wind-magnetosphere energy coupling function fitting: Results from a global MHD simulation, *J. Geophys. Res. Space Physics*, **119**, 6199–6212, doi:10.1002/2014JA019834.
- Wang, C.-P., L. R. Lyons, T. Nagai, J. M. Weygand, and R. W. McEntire (2007), Sources, transport, and distributions of plasma sheet ions and electrons and dependences on interplanetary parameters under northward interplanetary magnetic field, *J. Geophys. Res.*, **112**, A10224, doi:10.1029/2007JA012522.
- Wang, J., Q. Zhong, S. Liu, J. Miao, F. Liu, Z. Li, and W. Tang (2015), Statistical analysis and verification of 3-hourly geomagnetic activity probability predictions, *Space Weather*, **13**, 831–852, doi:10.1002/2015SW001251.
- Weimer, D. R. (2001), An improved model of ionospheric electric potentials including substorm perturbations and application to the Geospace Environment Modeling November 24, 1996, event, *J. Geophys. Res.*, **106**(A1), 407–416, doi:10.1029/2000JA000604.
- Wing, S., J. R. Johnson, J. Jen, C.-I. Meng, D. G. Sibeck, K. Bechtold, J. Freeman, K. Costello, M. Balikhin, and K. Takahashi (2005), K_p forecast models, *J. Geophys. Res.*, **110**, A04203, doi:10.1029/2004JA010500.
- Wing, S., J. R. Johnson, and M. Fujimoto (2006), Timescale for the formation of the cold-dense plasma sheet: A case study, *Geophys. Res. Lett.*, **33**, L23106, doi:10.1029/2006GL027110.
- Wygant, J. R., R. B. Torbert, and F. S. Mozer (1983), Comparison of S3-3 polar cap potential drops with the interplanetary magnetic field and models of magnetopause reconnection, *J. Geophys. Res.*, **88**, 5727–5735, doi:10.1029/JA088iA07p05727.